Article no. 21

THE CIVIL ENGINEERING JOURNAL 2-2020

GEOSPATIAL AND TEMPORAL ANALYSES OF RURAL AREA FOR VEGETATION ANALYSIS

Paulina Raeva and Karel Pavelka, Jr.

Czech Technical University in Prague, Faculty of Civil Engineering, Department of Geomatics, Prague, Thákurová 2077/7, Czech Republic; paulina.raeva@fsv.cvut.cz, karel.pavelka1@fsv.cvut.cz

ABSTRACT

The current paper aims at presenting multitemporal monitoring of two crop fields using close-range aerial photogrammetric techniques with a combination of different sensors. A fixed-wing unmanned aerial vehicle was used to map the crops regularly in 2016 and 2017. The goal of the following study is to show the experimental results of an enhanced keypoint number extraction of NIR and TIR images and the importance of radiometric calibration of close-range data.

KEYWORDS

RPAS, UAV, multispectral data, agriculture

INTRODUCTION

The progression of technology has resulted in technical devices taking over many human labours in our daily life routines. This fact could be, on one hand, worrying but on the other hand, prosperous for many specialities. The advent of unmanned aerial systems (UAS) was first in the military sector, likewise many other geodetic devices, such as GNSS receivers which we nowadays cannot do without. Therefore, UAS or also RPAS (Remotely Piloted Aircraft Systems) have made their presence significant in Geodesy, Photogrammetry and Geoinformatics. Nowadays, they play an important role in monitoring agriculture, forestry or archaeology.

Aircraft with a fixed-wing is primarily focused on mapping vast and flat fields [1], for example, agricultural ones, moreover, they are the preferable platform for multitemporal aerial mapping. According to European research [2], unmanned aircraft have the advantage to help farmers take better care of their filed and boost their yield. Bearing in mind the unstable weather conditions, the soil heterogeneity etc, farmers need a dynamic attitude toward atomization. As some others state [3] the RPAS is one of the possible ways to aid farmers in optimizing their profit and improve production.

STUDY AREA

Background of the study

This study began at the Department of Geomatics in 2016. It is a part of a project on mapping battlefield engravements built during the Thirty Years' War [4]. The RPAS mapping was provided to find remnants of an artillery camp fortification. Later, it was stated that these remnants are situated elsewhere but the imagery was used to evaluate the possible implementation of close-range multispectral photogrammetry in agriculture. The reason to carry our an agronomic survey was the information stated in the database LPIS that most of the fields suffer from a significant

percentage of soil erosion. The authors then reckoned that it would be challenging to trace problematic wet field spots with the help of a thermal infrared camera.

Location

The area of interest is nearby the village of Vysoke Sedliste (49.83ºN, 12.77ºE), in the Pilsen Region in the Czech Republic (Figure1 b). The average elevation is 570 m above sea level (Figure1 a).

Fig. 1(a,b) – a: DMS 1 generation, CUZK; b: test fields near Vysoke Sedliste

Crop description

In the current study, three crops were examined – spring barley, corn and winter wheat. The spring barley is usually planted in January. It does not need much watering because this may lead to decomposition of the crop. Spring barley grows in cool and dry areas and ripens for 60-70 days. Barley in the Czech Republic is harvested in the same period as wheat – July, August. The optimal growing conditions for winter wheat though are in high-drained soil.

The crop fields are situated in the cadastral territory of Vysoke Sedliste. Detailed information is taken from the Land Parcel Information System (LPIS). According to the Czech State Investment Fund for Agriculture [5] the crops cultivated in field №3304/7 (according to LPIS) in 2016 were barley, corn and triticale and in 2017 winter wheat and barley.

METHODS AND TECHNIQUES

Flight campaigns

We used the fixed-wing platform eBee which is at disposal at the Department of Geomatics. It is completely autonomous and flies according to a pre-set flight plan which is created in eMotion. The basics of the flight plan are: setting a take-off location, start waypoint and location for landing and home waypoints in case of emergency. The core of a good flight plan is to set the take-off location to be higher than the area to be mapped. Moreover, crucial for the take-off and landing location is to be set against the upcoming wind. The flight campaigns took place in April, June and July 2016 and 2017. Every month the area was mapped with both near-infrared (NIR) and thermal infrared (TIR) sensor.

Near-infrared camera

For better understanding the crop health, we used a 4-band multispectral sensor. It is the multiSPEC 4C modified professional. This camera can capture images outside of the visible electromagnetic spectrum, it produces images in green, red, red-edge and near infra-red parts of the spectrum. The central wavelengths of the bands are as follows: green – 550nm, red – 660 nm, red-edge 735nm and NIR – 790nm [6]. The full camera resolution is 1.2Mpx. The camera takes imagery only in TIFF. The multiSPEC 4C has an irradiance sensor on top of it which helps the pre-flight calibration process and enables providing with absolution reflectance measurements. Radiometric calibration was performed before each flight. For this purpose, a radiometric target was put horizontally on the ground and a few images were taken from a 50 cm distance. The radiometric target is captured in all four bands. These images were later used in the post-processing procedure.

Thermal infrared camera

For better understanding the relationship between soil and crops, a thermal mapping was performed. We used the thermoMAP by senseFly. This is an advanced professional imaging solution for solar, industrial and agronomic inspections. It is capable of capturing imagery between 7.5 and 13.,5 with a central wavelength – 10000.5 nm, the photo size is 640x512 pixels with 14 cm ground sampling distance (GCD) at 75 m flying altitude [7]. The capture rate is 7.5 photos per second or 7.5 frames per sec when shooting video footage. The scene temperature is between -40°C to 160°C with a temperature resolution of 0.1°C. This camera could be considered as an uncooled thermal infrared camera. The uncooled thermal cameras keep their temperature approximately equal to the ambient one, therefore, the temperature controlling system is simpler. These cameras base their system on bolometer technology.

DATA PROCESSING

The multispectral images were stored in 8bit TIFF with a resolution of 1280 x 960 with a focal length of 4mm. As the camera has four bands, four different folders were automatically created in the directory of the input imagery. Each of these folders contains the images from only one spectral band. We used Pix4Dmapper for our post-processing [8]. The software uses the Structure-from-Motion algorithm which searches for matching features in the dataset of overlapping digital images. The software automatically recognizes the band of each image. The thermal images were stored in 16bi TIFF with a resolution of 640 x 512 and a focal length of 9mm. The pixel values of the thermal images are stored in nanometers. Two processing templated were created for both image types. The difference is in the input values for keypoint extraction – 15 000 for NIR and 20 000 for TIR (Table 1 and Table 2). The important part for the camera calibration step with TIR is to opt for an alternative calibration pipeline which does not take into account obliques images with a Z angle larger than 35° based on the keypoint matching the software performs Automatic Aerial Triangulation (AAT) and Block Bundle Adjustment (BBA). The AAT is the process of determining X, Y and Z ground coordinates of the individual points based on the image coordinate measurements [9]. Figures 2 and 3 show the pixel errors, the average direction and magnitude of the reprojection error for each pixel. The number of automatically matched points is colour-coded between black and white. White indicates that more than 16 automatic points were extracted at the pixel location. Black, on the other hand, indicates that no points have been extracted. The number of extracted and match keypoints was computed. The maximum number of keypoints for NIR (20 000) was reached only in the green-band images. Images from red, red-edge and NIR bands produced a lower number of keypoints. The maximum number of keypoints extracted from TIR images was approximately 12 000. Therefore, enhancing this number did not improve the image pairs

matching. It is important to indicate the fact that all NIR and TIR images have vignetting meaning they have shaded or blur edges. The edge vignetting is caused by the lens itself.

Tab. 1 - Comparison of the number of image keypoints in all four bands. only the green-band images reached the set values – 15 000

	Green		Red		Red-Edge		NIR	
	Keypoints	Matching	Keypoints	Matching	Keypoints	Matching	Keypoints	Matching
Median	12265	6022	12859	6065	12128	3653	11976	3607
Min	11320	831	12362	1614	11525	1031	11441	711
Max	**15000**	7242	**13193**	7270	**12774**	5362	**12960**	5433
Average	12298	5663	12816	5718	12128	3669	12021	3510

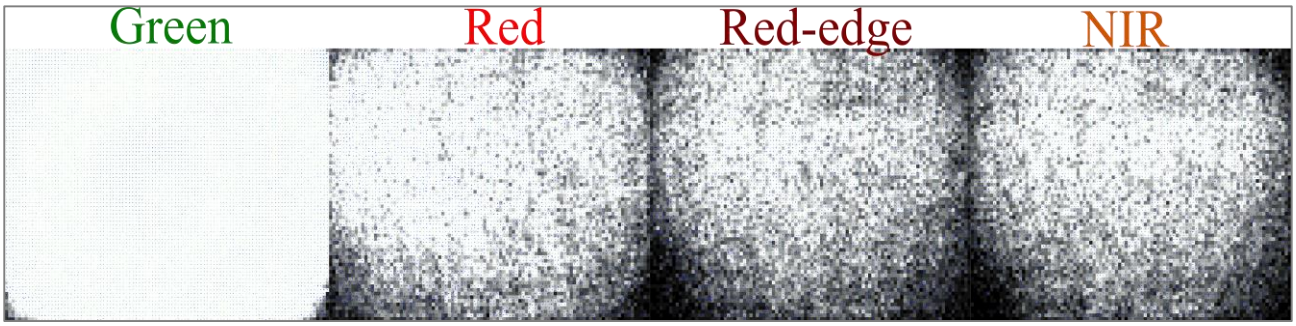

Fig. 2 – Keypoints extraction from all NIR band images. The white colour stands for more than 16 extractions and black – 0 extractions.

Tab. 2 - Number of keypoints extracted from the TIR images. The set value of 20 000 was not reached.

	IR	
	Keypoints	Matching
Medium	8387	3419
Min	5652	514
Max	**11178**	6253
Average	8405	3443

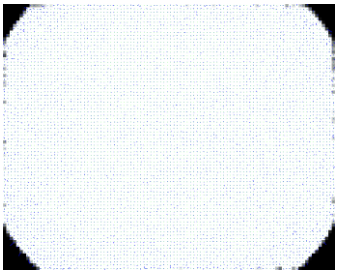

The Structure-from-Motion enables the formation of a sparse point cloud from all extracted and matched points. The sparse pointcloud serves as a base for the creation of a dense pointcloud. The average point number and density for the NIR projects is 9 mil. and 3 points [m^3] and for the TIR – 7mil and 2 points [m^3].

Creating DSM and Reflectance Maps

To create a Digital Surface Model (DSM), the dense pointcloud is used as a base. By default, the DSM is created with the same GSD resolution. The multispectral datasets resulted in a GSD of approximately 16cm/pix and the thermal ones – 20÷21 cm/pix. In this study, no orthophoto maps were created but reflectance maps instead. These two are quite similar in computation as both are corrected for perspective and the pixel values are obtained as a weighted average of the

pixels in the original images, corresponding to the particular pixel. Each reflectance pixel map represents the object reflectance or in other words, the pixel values are the values of the electromagnetic wavelengths.

To create a corrected reflectance map, one must apply radiometric corrections, especially when using a modified multispectral camera and comparing multitemporal datasets. Every object could be characterized with a spectral reflectance ρ (λ) which could be defined as a ration between the intensity of the reflectance energy Mr and the intensity of the incident one M_i for a certain wavelength (λ)[10]:

$$\rho(\lambda) = \frac{M_r(\rho)}{M_i(\rho)} . 100\ [\%] \quad (1)$$

The reflectance values for the 4-band multispectral camera are given in Table 3.

Tab. 3 - Reflectance values of the radiometric panel for all camera bands

Green	17.12%	0.1712
Red	20.32%	0.2032
Red-Edge	24.68%	0.2468
NIR	35.13%	0.3513

The reflectance R [%] is computed according to (2) where DN stands for 'digital number', i – band and a, b are coefficients.

$$R = a_i DN + b_i \quad (2)$$

Index Maps

Thanks to the different spectral bands and the combinations between them, the so-called vegetation indices VI were computed. There are many types of VI classifications but for the current study, a few VI were used which are classified as ration VI.

The Normalized Difference Vegetation Index was applied to all multispectral imagery. The NDVI relates to the green biomass during vegetation growth. It relates to the difference between the reflected energy in the NIR and red part of the electromagnetic spectrum. The formula is as follows [11]:

$$NDVI = \frac{\rho_{NIR} - \rho_{RED}}{\rho_{NIR} + \rho_{RED}} \quad (3)$$

The second we computed is the Green Normalized Difference Index which is quite similar to the previous one. It uses the reflected energy in the green part of the spectrum instead of the red one. It is more sensitive to chlorophyll in the plants. The formula is as follows:

$$GNDVI = \frac{\rho_{NIR} - \rho_{GREEN}}{\rho_{NIR} + \rho_{GREEN}} \quad (4)$$

Moreover, we can calculate another important VI thanks to the multiSPEC 4c camera. This the normalized Difference Red-Edge Index (NDRE). This VI indicates the rapid change in vegetation reflectance between the visible and infrared light. NDRE is also sensitive to chlorophyll in plants. Its formula is:

$$NDRE = \frac{\rho_{NIR} - \rho_{RED-EDGE}}{\rho_{NIR} + \rho_{RED-EDGE}} \quad (5)$$

Last, but by no means, the least important index calculated is the temperature index TI. It is nor used very often in agriculture, but it gives relevant information about the soil moisture. As

stated in the description, the study fields are prone to erosion. In this case, it is essential to map the field with a thermal camera. The thermal reflectance maps contain information about the reflectance not only from the crop surface but also from the soil in case of sparse vegetation. Moreover, the electromagnetic waves of the camera are longer which provides reflectance even from beneath the soil. This information is converted into Celsius, according to the formula:

$$Temp\ [oC] = 0.01 * ref.value - 100, \quad (6)$$

Where ref. value stands for the reflectance values in each pixel.

RESULTS

The results of the computation are index maps with the same colour-scheme for better understanding the crop changes in time. In Figure 4 we showed a comparison of NDVI and TI index of the spring barley for April and June 2016 and 2017. Problematic spots show similar behaviour during both years (indicated in a circle), e.g. the lower the NDVI the hight the temperature. This could mean either sparse vegetation or problematic soil pattern.

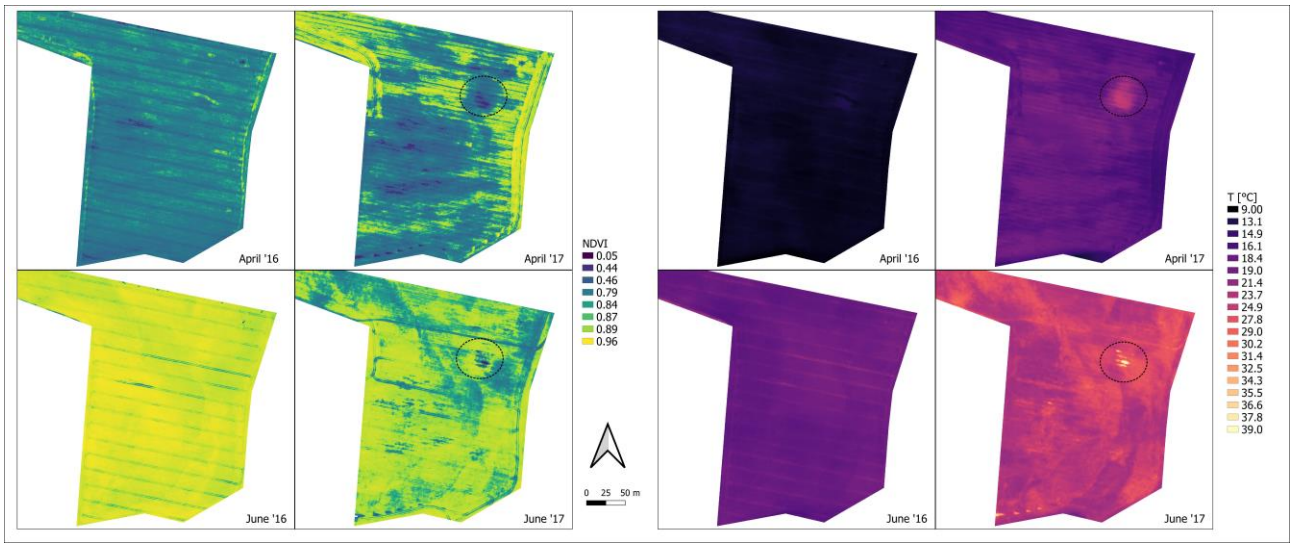

Fig. 3 – Comparison between NDVI and TI maps from 2016 and 2017 for spring barley. Spots with similar behaviour are indicated in a circle.

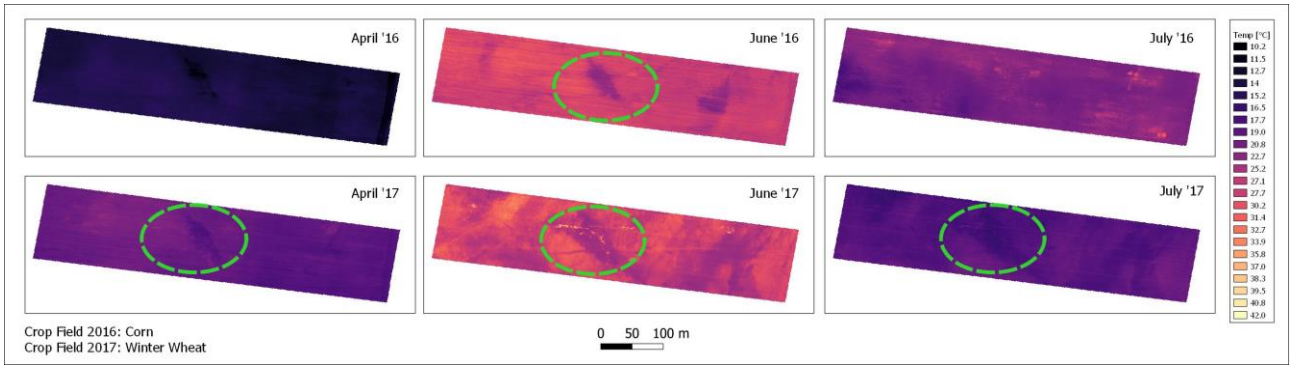

Fig. 5 – Comparison between TI maps from 2016 and 2017 for corn and winter wheat. Spots with similar behaviour are indicated in a circle.

The TI maps for the cornfield are shown in Figure 5. Again, it was noticed a spot which remains problematic during both years. The spot shows a lower temperature than its surroundings. We prepared a histogram comparison for the spring barely field for July 2017 in order to study the distribution of index values (Figure 6). We also added a SAVI (Soil Adjusted Vegetation Index) to the comparison.

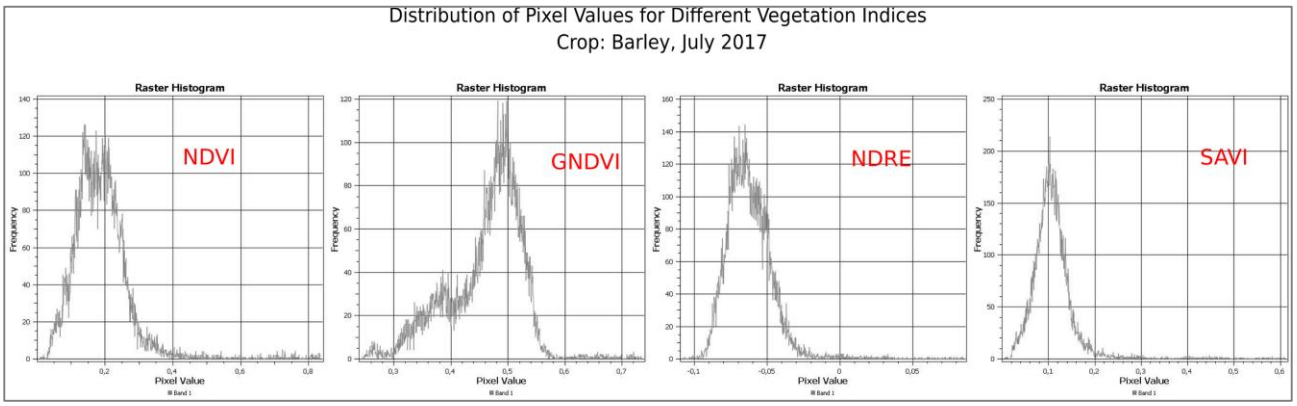

Fig. 6 – Distribution of pixel values for different vegetation indices – NDVI, GNDVI, NDRE and SAVI. The evaluated crop is spring barely in July 2017 – before harvesting.

EXPERIMENTS

This experiment is based on the importance of the radiometric calibration of the NIR images Thus, two datasets of the cornfield were computed with no radiometric calibration and the NDVI values were compared. The datasets are from June and August 2016. The results for the crop field in June are:

Tab. 4 - Comparison of calibrated and non-calibrated DN for June 2016 – a cornfield

Cornfield June 2016	minNDVI	modeNDVI	maxNDVI	Stand. Deviation σ
Calibration	0,33	0,43	0,90	0.03
No Calibration	0,14	0,25	0,86	0.04

Tab. 5 - Comparison of calibrated and non-calibrated DN for August 2016 - a cornfield

Cornfield August 2016	minNDVI	modeNDVI	maxNDVI	Stand. Deviation σ
Calibration	0,47	0,95	0,96	0.02
No Calibration	0,31	0,91	0,94	0.03

MinNDVI stands for the minimum values, mode – the most frequent value and max – the maximum values.

ANALYSES AND DISCUSSION

The theoretical background seems easy to apply in close-range photogrammetry techniques. Unfortunately, this is not the case as one have to deal with preparing a current pre-

flight plan with bigger overlap than the theoretical 60% lateral and 80% longitudinal as applied in classic aerial photogrammetry. Mapping with a TIR camera like thermoMAP means providing a 90% overlap in both sides as the resolution is quite low and the post-processing, namely, camera calibration requires a certain amount of perpendicular to the terrain photographs. The same applies to the NIR multispectral cameras. Another challenge is the post-processing of the great amount of imagery. At first attempts. Not all NIR or TIR images were oriented. That is why in this study, we opted for an enhanced number of keypoints. The results show that 15 000 keypoints can be extracted only from the green-band photographs. And with these apriori value, the extracted points from the other bands (red, red-edge and NIR) are approximately around 10 000. The case is similar to computing TIR images. We have chosen to extract 20 000 keypoints, because of low image resolution means fewer matches between the images. Unfortunately, the maximum number of extracted keypoints was 12 000. Nonetheless, the challenge of processing TIR images were not over. Correct computation of a reflectance map is possible only when the camera positions are calibrated with an alternative pipeline method. This method, though, excludes oblique photos with more than 35-degree rotation. This is the reason why a large number of TIR were automatically ignored while processing. Any other calibration methods lead to ambiguities and distorted relative models. After computing the Bundle Block Adjustment with the NIR and TIR datasets, it was noticed the presence of lens vignetting. This leads to no point extraction from the image edges. Removing the vignetting from the TIR images will be a goal in our future work.

We experimented to test the importance of radiometric calibration of the DN when dealing with multitemporal monitoring of the same area. The results indicate differences between the calibration and non-calibrated values. Despite the fact, the maximum values are practically the same, the biggest difference are notices in the minimum and mode values.

We created statistical models in order to combine all the information from the VI computation. The graphical results may be sometimes misleading for people outside of the Remote Sensing sphere. Farmers should be provided with statistical analyses to better plan the future vision of their digital farms. Figure 7 shows the development of the spring barley field for 2016 and 2017 in months April, June and July.

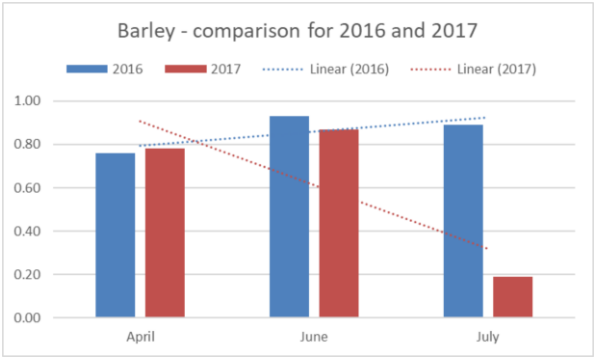

Fig. 7 – Comparison of NDVI values from 2016 and 2017 for spring barley.

The similar behaviour between NDVI and TI in problematic spots was noticeable, for instance in Figure 3. These spots may be due to dry erosion. The correlation and dependence of these two indices could be simply explained with the fact that the soil similarly reflects electromagnetic light in both NIR and TIR parts of the spectrum.

An overall comparison of all computed VI for the same field is shown in Figure 8. In 2016 its cultivated crop was corn and in 2017 – winter wheat.

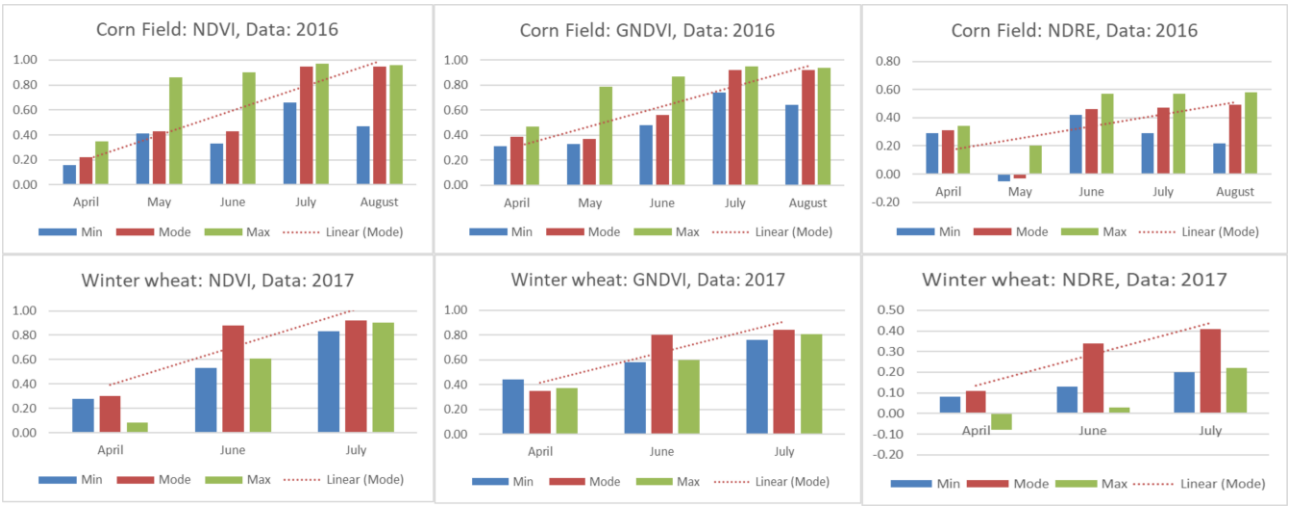

Fig. 8 – Development of the same field with two difference crops – corn (2016) and winter wheat (2017)

Future work for the authors will be to explain this correlation statistically with more data from different sensors. Future experiments will also include computing VI resist to soil refraction, e.g. SAVI (Soil Adjusted Vegetation Index) and seek for correlation between VI and TI. According to Figure 6 SAVI values are similar to the normal distribution. Moreover, NDVI and SAVI use the same spectral bands which means SAVI could be a more reliable index for multispectral close-range photogrammetric analyses

ACKNOWLEDGEMENTS

This paper is part of the project 161 -1612053A155 Development and Application of Modern Devices and Techniques for Spatial Data Acquisition, Processing, Analysis and Visualization funded by the Czech Technical University in Prague.

REFERENCES

[1] K. Pavelka, J. Šedina, J. Pacina, L. Plánka, J. Karas, and V. Šafář, *RPAS Remotely Piloted Aircraft System*. Prague: České vysoké učení technické v Praze, 2016.
[2] SESAR Joint Undertaking, “European Drones Outlook Study,” no. November, p. 93, 2016.
[3] J. Lukáš *et al.*, “Využití bezpilotních prostředků v zemědělství 1.část,” 2016.
[4] T. Janata, “Research Project on Engraving of the Thirty Years’ War Battlefields,” *Geodetický a kartografický obzor*, Prague, p. 7, 2018.
[5] SZIF, “Státní zemědělský intervenční fond,” 2020. [Online]. Available: https://www.szif.cz/en?setCookie=true.
[6] SenseFly Ltd, *multiSPEC 4C CameraUser Manual*, no. February. 2017.
[7] SenseFly Ltd, *thermoMAP Camera*. 2017.
[8] Pix4D, *Pix4Dmapper 4.1 User Manual*. Lausanne, 2020.
[9] P. R. Wolf, B. A. Dewitt, and B. E. Wilkinson, *Elements of Photogrammetry with Applications in GIS*. McGraw-Hill Education, 2014.
[10] L. Halounová and K. Pavelka, “Dálkový průzkum Země,” p. 182, 2008.
[11] J. W. Rouse, R. H. Haas, J. A. Schell, D. W. Deering, and J. C. Harlan, “Monitoring the Vernal Advancement and Retrogradation (Greenwave effect) of Natural Vegetation,” 1974.